Comput Mech (2005) 36: 360–374
DOI 10.1007/s00466-005-0659-4

ORIGINAL PAPER

E. E. Tzirtzilakis · V. C. Loukopoulos

Biofluid flow in a channel under the action of a uniform localized magnetic field

Received: 11 July 2004 / Accepted: 17 January 2005 / Published online: 6 July 2005

Abstract In this work the fundamental problem of the biomagnetic (blood) fluid flow in a channel under the influence of a steady localized magnetic field is studied. For the mathematical formulation of the problem both magnetization and electrical conductivity of blood are taken into account and blood is considered as a homogeneous Newtonian fluid. For the numerical solution of the problem, which is described by a coupled, non linear system of PDEs, with appropriate boundary conditions, the stream function–vorticity formulation is adopted. The solution is obtained by the development of an efficient numerical technique based on finite differences. Results concerning the velocity and temperature field, skin friction and rate of heat transfer, indicate that the presence of the magnetic field influences considerably the flow field. It is also obtained that the electrical conductivity of blood should be taken into account at the area of the uniform magnetic field.

List of symbols

H	magnetic field strength (A m^{-1})
B	magnetic field induction ($B = \mu_o H$) (Tesla)
T	temperature (K)
T_u	temperature of upper plate
T_l	temperature of lower plate
L	length of plates (m)
h	distance between plates (m)
(x, y)	components of the cartesian system
(u, v)	velocity components
p	pressure
ρ	fluid density (kg m^{-3})
σ	electrical conductivity (S m^{-1})
μ	dynamic viscosity (kg m^{-1} s^{-1})
μ_o	magnetic permeability of vacuum (H m^{-1})
c_p	specific heat at constant pressure (J kg^{-1} K^{-1})
k	thermal conductivity (J $m^{-1}s^{-1}$ K^{-1})
M	magnetization of the fluid (A m^{-1})
K	constant
T_c	Curie temperature
a_1, a_2	constants
u_r	maximum velocity at the entrance (m s^{-1})
$J = J(x, y)$	vorticity function
$\Psi = \Psi(x, y)$	stream function
Re	Reynolds number
Pr	Prandtl number
Ec	Eckert number
ϵ	temperature number
Mn_F	magnetic number (FHD)
Mn_M	magnetic number (MHD)

E. E. Tzirtzilakis (✉)
Department of Mathematics,
University of Partas,
26500 Patras, Greece
E-mail:tzirtzi@iconography.gr

V. C. Loukopoulos
Department of Physics,
University of Partas,
26500 Patras, Greece

1 Introduction

A Biomagnetic fluid is a fluid that exists in a leaving creature and its flow is influenced by the presence of magnetic field. The study of the flow of a biological fluid under the influence of a magnetic field is investigated recently by many researchers due to the applications which seem to be numerous in bioengineering and medicine [1–7]. The most characteristic biomagnetic fluid is blood, which behaves as a magnetic fluid, due to the complex interaction of the intercellular protein, cell membrane and the haemoglobin, a form of iron oxides, which is present at a uniquely high concentration in the mature red blood cells. Moreover, its magnetic property is affected by factors such as the state of oxygenation.

The first who reported that the erythrocytes orient with their disk plane parallel to the magnetic field where Pauling and Coryell. They also found that blood possesses the property of diamagnetic material when oxygenated and paramagnetic when deoxygenated [8]. Since then, several investigators studied the orientation of erythrocytes in magnetic fields of strength 1–8 Tesla [9–11]. Moreover, it was found that other cells of blood, except the erythrocytes, like platelets, also orient with the applied magnetic field [12].

In order to investigate the flow of a biomagnetic fluid under the action of an applied magnetic field Haik et al. developed the mathematical model of Biomagnetic fluid dynamics (BFD) [4, 13, 14]. They considered blood as a non electrically conducting fluid and derived the mathematical model based on the principles of Ferro hydro dynamics (FHD) [15–21].

Primary role in FHD, and thus in BFD, plays the magnetization M of the biofluid. The magnetization is a quantity which expresses how much the magnetic field affects the magnetic fluid and generally is a function of the magnetic field intensity H and the temperature T.

Thus, unlike "Magnetohydrodynamics" (MHD), which deals with conducting fluids, the aforementioned mathematical model of BFD, ignores the effect of polarization and magnetization and the induced current is negligibly small. In that model of BFD, unlike MHD, Lorentz force is much smaller in comparison to the magnetization force.

The magnetization force depends on the existence of a spatially varying magnetic field. According to the above mentioned mathematical model, biofluids are considered as poor conductors and the flow is affected only by the magnetization of the fluid in a spatially varying magnetic field.

However, blood in particular, exhibits considerably high static electrical conductivity, hematocrit and temperature dependence. Moreover, the electrical conductivity of blood varies as the flow rate varies [22–24]. Consequently, in order to investigate the effect of a localized uniform magnetic field on an electrically conducting biofluid, like blood, it is necessary to include into the mathematical model of BFD the arising Lorentz force as it happens in MHD [25–27].

As the biofluid enters and leaves the locally applied magnetic field, where the gradient of the magnetic field strength is high, the force due to magnetization arises, whereas, in the region inside of which the magnetic field is uniform, the Lorentz force prevails. In the present study the mathematical model of BFD is extended, using the principles of MHD, in order to include the effect of the electrical conductivity of blood under an applied magnetic field. This model of BFD is used to obtain numerical results regarding the fluid flow (blood) in a rectangular channel under the action of a localized uniform magnetic field.

The flow is assumed to be two dimensional, laminar, incompressible and the magnetization is described by a linear equation involving the magnetic intensity H and the temperature T. The two impermeable plates of the channel are kept at different constant temperatures and as far as the magnetic field is concerned, equilibrium flow is assumed. The biofluid is blood and it is considered as a homogeneous and Newtonian fluid (flow in large vessels) as in [28, 29]. The above mentioned simplifications may not be very realistic but are appropriate for a first understanding of the physical problem under consideration.

In order to proceed to the numerical solution of the coupled, non linear system of PDEs involved in the model used in the present paper, the stream function–vorticity formulation is adopted and the solution of the problem is obtained numerically by the development of an efficient numerical technique using finite differences. This technique assures that in the algebraic system arising after the discretization, the matrix of the unknowns is diagonally dominant.

The results concerning the velocity and temperature field, skin friction and rate of heat transfer presented, show that the flow is influenced considerably by the magnetic field. The major effect is the formation of two vortices which arise at the areas where the magnetic field starts and stops to apply. The temperature is also increasing within the area where the magnetic field is applied. These results indicate that the application of a magnetic field, in the flow of a biomagnetic fluid, could be useful for medical and engineering applications.

2 Mathematical Formulation

The viscous, steady, two-dimensional, incompressible, laminar biomagnetic fluid (blood) flow is considered taking place between two parallel flat plates (channel). The length of the plates is $\bar{L}$ and the distance between them is $\bar{h}$. The flow at the entrance is assumed to be fully developed and the upper plate is kept at a constant temperature $\bar{T}_{\mathrm{u}}$, while the lower at $\bar{T}_{\mathrm{l}}$, such that $\bar{T}_{\mathrm{l}} < \bar{T}_{\mathrm{u}}$. The origin of the Cartesian coordinate system is located at the leading edge of the lower plate. The flow is subject to a locally applied uniform magnetic field, which is placed between the points $(\bar{x}_1, 0)$ and $(\bar{x}_2, 0)$ and acts perpendicularly to the x direction (see Fig. 1).

As already mentioned in the introduction, the BFD model of Haik et al. [4, 13, 14] does not take into consideration the electrical conductivity of blood. However, the Lorentz force, which is due to the electrical conductivity of blood, is not negligible in the region where the uniform magnetic field is applied and should be taken under consideration. Theoretically, as the biofluid enters and leaves the locally applied magnetic field, where the gradient of the magnetic field strength is high, the force due to magnetization as well as the Lorentz force arise. In the region inside of which the magnetic field is uniform the Lorentz force prevails and the magnetization force becomes zero. Also, due to the way the magnetic field is applied, the gradient of the magnetic field strength exists only along the x direction, whereas is zero along the y direction. The Lorentz force will arise due to the velocity component u which is transverse to the magnetic field.

Blood is considered as a homogeneous, electrically conducting biomagnetic fluid and Newtonian behavior

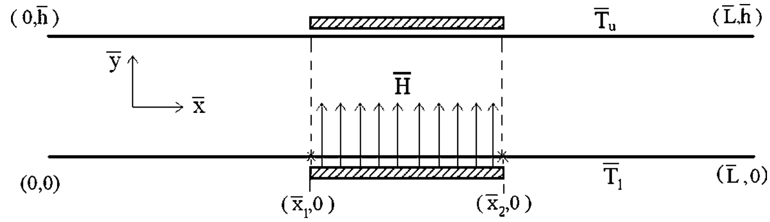

Fig. 1 Flow domain, the uniform magnetic field of strength $\bar{H}$ is applied between the points $\bar{x}_1$ and $\bar{x}_2$

is assumed. The rotational forces acting on the erythrocytes when entering and leaving the magnetic field are discarded (equilibrium magnetization). This assumption, even though it is a simplification, is very close to reality and experiments show that is valid for blood [14].

At the channel flow, under the above assumptions, the dimensional velocity components of $\vec{q}=(\bar{u},\bar{v})$, the pressure $\bar{p}$ and the temperature $\bar{T}$, are governed by the mass conservation, the fluid momentum equations at the $\bar{x}$, $\bar{y}$ directions, and the energy equation, which are given respectively by

$$\frac{\partial \bar{u}}{\partial \bar{x}} + \frac{\partial \bar{v}}{\partial \bar{y}} = 0, \tag{1}$$

$$\bar{\rho}\left(\bar{u}\frac{\partial \bar{u}}{\partial \bar{x}} + \bar{v}\frac{\partial \bar{u}}{\partial \bar{y}}\right) = -\frac{\partial \bar{p}}{\partial x} + \bar{\mu}_0 \bar{M}\frac{\partial \bar{H}}{\partial \bar{x}} - \bar{\sigma}\bar{B}^2\bar{u} + \bar{\mu}\left(\frac{\partial^2 \bar{u}}{\partial \bar{x}^2} + \frac{\partial^2 \bar{u}}{\partial \bar{y}^2}\right), \tag{2}$$

$$\bar{\rho}\left(\bar{u}\frac{\partial \bar{v}}{\partial \bar{x}} + \bar{v}\frac{\partial \bar{v}}{\partial \bar{y}}\right) = -\frac{\partial \bar{p}}{\partial \bar{y}} + \bar{\mu}\left(\frac{\partial^2 \bar{v}}{\partial \bar{x}^2} + \frac{\partial^2 \bar{v}}{\partial \bar{y}^2}\right), \tag{3}$$

$$\bar{\rho}\bar{c}_p\left(\bar{u}\frac{\partial \bar{T}}{\partial \bar{x}} + \bar{v}\frac{\partial \bar{T}}{\partial \bar{y}}\right) + \bar{\mu}_0\bar{T}\frac{\partial \bar{M}}{\partial \bar{T}}\left(\bar{u}\frac{\partial \bar{H}}{\partial \bar{x}} + \bar{v}\frac{\partial \bar{H}}{\partial \bar{y}}\right) - \bar{\sigma}\bar{B}^2\bar{u}^2 = \bar{k}\left(\frac{\partial^2 \bar{T}}{\partial \bar{x}^2} + \frac{\partial^2 \bar{T}}{\partial \bar{y}^2}\right) + \bar{\mu}\left[2\left(\frac{\partial \bar{u}}{\partial \bar{x}}\right)^2 + 2\left(\frac{\partial \bar{v}}{\partial \bar{y}}\right)^2 + \left(\frac{\partial \bar{v}}{\partial \bar{x}} + \frac{\partial \bar{u}}{\partial \bar{y}}\right)^2\right]. \tag{4}$$

The boundary conditions of the problem are

$$\left.\begin{array}{lll} \text{Inflow} & (\bar{x}=0, 0\le\bar{y}\le\bar{h}): & \bar{u}=\bar{u}(\bar{y}), \bar{v}=0, \\ & & \bar{T}=\bar{T}(\bar{y}) \\ \text{Outflow} & (\bar{x}=\bar{L}, 0\le\bar{y}\le\bar{h}): & \partial(\bar{R})/\partial\bar{x}=0 \\ \text{Upper plate} & (\bar{y}=\bar{h}, 0\le\bar{x}\le\bar{L}): & \bar{u}=0, \bar{v}=0, \bar{T}=\bar{T}_{\mathrm{u}} \\ \text{Lower plate} & (\bar{y}=0, 0\le\bar{x}\le\bar{L}): & \bar{u}=0, \bar{v}=0, \bar{T}=\bar{T}_l \end{array}\right\}. \tag{5}$$

In the above equations $\bar{u}(\bar{y})$ is a parabolic velocity profile corresponding to the fully developed flow, $\bar{T}(\bar{y})$ is a linear profile, $\bar{R}$ stands for $\bar{T}$, $\bar{u}$ or $\bar{v}$, $\bar{\rho}$ is the biomagnetic fluid density, $\bar{\sigma}$ is the electrical conductivity, $\bar{\mu}$ is the dynamic viscosity, $\bar{\mu}_o$ is the magnetic permeability of vacuum, $\bar{c}_p$ is the specific heat at constant pressure, $\bar{k}$ is the thermal conductivity, $\bar{T}$ is the temperature, $\bar{H}$ is the magnetic field strength, $\bar{B}$ is the magnetic induction $(\bar{B}=\bar{\mu}_o\bar{H})$ and the bar above the quantities denotes that they are dimensional.

The term $\bar{\mu}_o\bar{M}\partial\bar{H}/\partial\bar{x}$ in (2), represents the component of the magnetic force, per unit volume, and depends on the existence of the magnetic gradient. The term $\bar{\mu}_0\bar{T}\frac{\partial\bar{M}}{\partial\bar{T}}\left(\bar{u}\frac{\partial\bar{H}}{\partial\bar{x}} + \bar{v}\frac{\partial\bar{H}}{\partial\bar{y}}\right)$ in (4), represents the thermal power per unit volume due to the magnetocaloric effect. These two terms arise due to the FHD [15–21].

The term $\bar{\sigma}\bar{B}^2\bar{u}$ appearing in (2), represents the Lorentz force per unit volume and arises due to the electrical conductivity of the fluid, whereas the term $\bar{\sigma}\bar{B}^2\bar{u}^2$ in (4) represents the Joule heating. These two terms arise due to the MHD [25–27].

For the variation of magnetization $\bar{M}$, with the magnetic field intensity $\bar{H}$ and temperature $\bar{T}$, the following relation derived experimentally in [30] is considered

$$\bar{M} = \bar{K}\bar{H}(\bar{T}_{\mathrm{c}} - \bar{T}), \tag{6}$$

where $\bar{K}$ is a constant and $\bar{T}_{\mathrm{c}}$ is the Curie temperature.

The magnetic field strength intensity H is considered to be independent of y and is given by the expression

$$\bar{H}(x,y) = \frac{\bar{H}_o}{2}(\tanh[a_1(\bar{x}-\bar{x}_1)] - \tanh[a_2(\bar{x}-\bar{x}_2)]), \tag{7}$$

where $\bar{H}_o$ is the magnetic field strength determined by the applied magnetic induction $(\bar{B}=\bar{\mu}_o\bar{H}_o)$ and x_1, x_2 are the points between of which the magnetic field is applied (see Fig. 1). Consequently, the magnetic field vector is $\bar{B}=(0,\bar{B},0)$. The coefficients a_1 and a_2 determine the magnetic field gradient at the points x_1 and x_2, respectively (see Fig. 2).

3 Transformation of equations

In order to proceed to the numerical solution of the system (1)–(4) with boundary conditions (15) and the assumptions (6) and (7), the following non dimensional variables are introduced

$$x = \frac{\bar{x}}{\bar{h}}, \quad y = \frac{\bar{y}}{\bar{h}}, \quad u = \frac{\bar{u}}{\bar{u}_r}, \quad v = \frac{\bar{v}}{\bar{u}_r}, \tag{8}$$

$$p = \frac{\bar{p}}{\rho\bar{u}_r^2}, \quad H = \frac{\bar{H}}{\bar{H}_o}, \quad T = \frac{\bar{T}-\bar{T}_l}{\bar{T}_u - \bar{T}_l}, \tag{9}$$

where $\bar{u}_r$ is the maximum velocity of blood at the entrance of the channel.

For the numerical solution, the stream function–vorticity formulation is adopted by introducing the

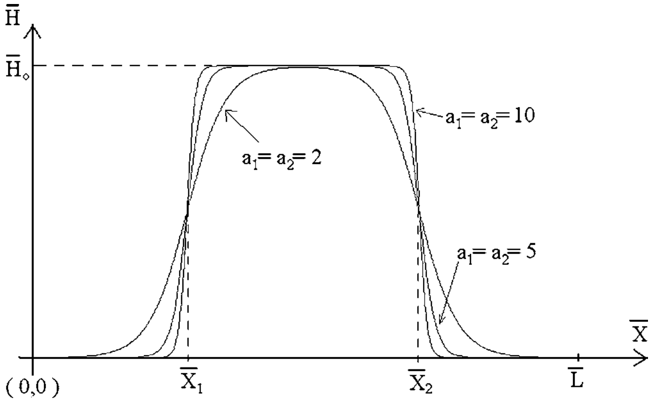

Fig. 2 Magnetic field of strength $\bar{H}$ with $\bar{x}$ for different a_1 and a_2

dimensionless vorticity function $J = J(x, y)$ and the dimensionless stream function $\Psi = \Psi(x, y)$ defined by the expressions

$$J(x, y) = \frac{\partial v}{\partial x} - \frac{\partial u}{\partial y}, \tag{10}$$

$$u = \frac{\partial \Psi}{\partial y}, \ v = -\frac{\partial \Psi}{\partial x}. \tag{11}$$

Thus, Eq. (1) is automatically satisfied and Eq. (2), (3) and (4) produce, by eliminating the pressure p from the first two and substituting (11) in (4) and (10), the following system of equations

$$\nabla^2 \Psi = -J, \tag{12}$$

$$\nabla^2 J = \text{Re}\left\{\frac{\partial J}{\partial x}\frac{\partial \Psi}{\partial y} - \frac{\partial J}{\partial y}\frac{\partial \Psi}{\partial x}\right\} - \text{Mn}_F \text{Re H}\frac{\partial H}{\partial x}\frac{\partial T}{\partial y} - \text{Mn}_M \text{H}^2 \frac{\partial^2 \Psi}{\partial y^2}, \tag{13}$$

$$\begin{aligned}\nabla^2 T = {} & \text{Pr Re}\left\{\frac{\partial T}{\partial x}\frac{\partial \Psi}{\partial y} - \frac{\partial T}{\partial y}\frac{\partial \Psi}{\partial x}\right\} \\ & + \text{Mn}_F \text{Pr Re Ec H}(\varepsilon + T)\left\{\frac{\partial H}{\partial x}\frac{\partial \Psi}{\partial y}\right\} \\ & + \text{Mn}_M \text{Pr Ec} H^2 \left\{\frac{\partial \Psi}{\partial y}\right\}^2 \\ & + \text{Pr Ec}\left\{\left(\frac{\partial^2 \Psi}{\partial y^2} - \frac{\partial^2 \Psi}{\partial x^2}\right)^2 + 4\left(\frac{\partial^2 \Psi}{\partial x \partial y}\right)^2\right\}.\end{aligned} \tag{14}$$

where ∇^2 is the two dimensional Laplacian operator $\left(\nabla^2 = \vec{\nabla} \cdot \vec{\nabla} = (\partial^2/\partial x^2 + \partial^2/\partial y^2)\right)$.

The non–dimensional parameters entering now into the problem under consideration are

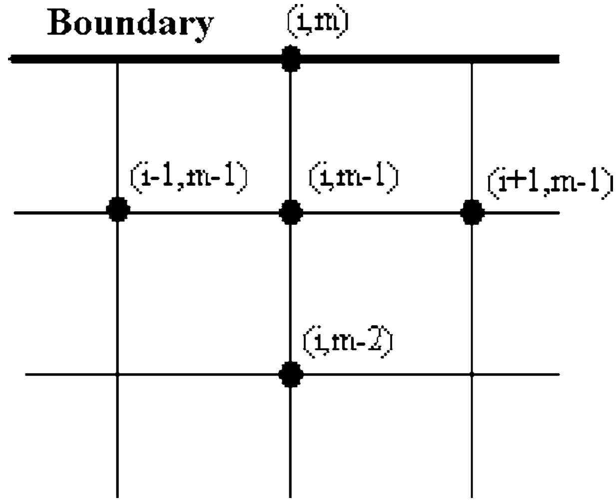

Fig. 3 Grid points for the calculation of $J_{i,m}$ at the boundary point (i, m)

$$\text{Re} = \frac{\bar{h}\bar{\rho}\bar{u}_r}{\bar{\mu}} \text{(Reynolds number)},$$

$$\text{Ec} = \frac{\bar{u}_r^2}{\bar{c}_p(\bar{T}_u - \bar{T}_l)} \text{(Eckert number)},$$

$$\varepsilon = \frac{\bar{T}_l}{\bar{T}_u - \bar{T}_l} \text{(Temperature number)},$$

$$\text{Pr} = \frac{\bar{c}_p \bar{\mu}}{\bar{k}} \text{(Prandtl number)},$$

$$\text{Mn}_F = \frac{\bar{\mu}_o \bar{H}_o^2 \bar{K}(\bar{T}_u - \bar{T}_l)}{\bar{\rho}\bar{u}_r^2}$$

(Magnetic number arising from FHD).

$$\text{Mn}_M = \frac{\bar{\mu}_o^2 \bar{H}_o^2 \bar{h}^2 \bar{\sigma}}{\bar{\mu}} \text{(Magnetic number arising from MHD)}.$$

The new parameters entering into the problems of BFD are the two magnetic numbers, Mn_F and Mn_M, defined above. It is worth mentioning here that when both these magnetic numbers are zero the problem is reduced to the problem of a common hydrodynamic flow in a channel with heat transfer. Also, for a specific Reynolds number and temperature difference, increasing these magnetic numbers is equivalent to increasing the magnetic field strength $\bar{H}_o$.

3.1 Boundary Conditions

The boundary conditions are implemented following [31] and they are

$$\left.\begin{array}{lll} \text{Inflow} & (x = 0, 0 \le y \le 1): & \Psi = 2y^2 - (4/3)y^3, \quad T = y, \quad J = 8y - 4 \\ \text{Outflow} & (x = \bar{L}/\bar{h}, 0 \le y \le 1): & \partial\Psi/\partial x = \partial T/\partial x = \partial J/\partial x = 0 \\ \text{Upper plate} & (y = 1, 0 \le x \le \bar{L}/\bar{h}): & \Psi = 2/3, \quad T = 1, \quad J = J_{i,m} \\ \text{Lower plate} & (y = 0, 0 \le x \le \bar{L}/\bar{h}): & \Psi = 0, \quad T = 0, \quad J = J_{i,m} \end{array}\right\} \tag{15}$$

where $J_{i,m}$ is an arbitrary boundary grid point at the plate calculated by the relation

$$J_{i,m} = -\frac{\left(\Psi_{i+1,m-1} - 2\Psi_{i,m-1} + \Psi_{i-1,m-1}\right)}{(\Delta x)^2} - \frac{\left(\Psi_{i,m-2} - \Psi_{i,m-1}\right)}{3(\Delta y)^2}. \quad (16)$$

4 Numerical method

For the numerical solution of the system of Eq. (12–14) an efficient technique has been developed based on a numerical method described in [31–33].

For the demonstration of the used numerical technique Eq. (13) is taken into account

$$\nabla^2 J = \mathrm{Re}\left\{\frac{\partial J}{\partial x}\frac{\partial \Psi}{\partial y} - \frac{\partial J}{\partial y}\frac{\partial \Psi}{\partial x}\right\} - \mathrm{Mn}_F \mathrm{Re}\ \mathrm{H}\frac{\partial H}{\partial x}\frac{\partial T}{\partial y} - \mathrm{Mn}_M\ \mathrm{H}^2\frac{\partial^2 \Psi}{\partial y^2}. \quad (17)$$

Equation (17) can be split into two equations, namely

$$\frac{\partial^2 J}{\partial x^2} - \mathrm{Re}\ u\frac{\partial J}{\partial x} = G_1(x,y) + A(x,y), \quad (18)$$

$$\frac{\partial^2 J}{\partial y^2} - \mathrm{Re}\ v\frac{\partial J}{\partial y} = -A(x,y), \quad (19)$$

where, $A(x,y)$ is an unknown function and

$$G_1(x,y) = -\mathrm{Mn}_F \mathrm{Re}\ \mathrm{H}\ \frac{\partial H}{\partial x}\frac{\partial T}{\partial y} - \mathrm{Mn}_M \mathrm{H}^2\frac{\partial^2 \Psi}{\partial y^2}$$

The next step is to consider the local transformation for Eq. (18) for $x_0 - \Delta x \le x \le x_0 + \Delta x$ and $y = y_0$:

$$J(x,y_0) = P(x,y_0)\mathrm{e}^{[-c(x,y_0)]},\ \text{where } c(x,y_0) = -\frac{\mathrm{Re}}{2}\int_{x_0}^{x} u(x,y_0)\,\mathrm{d}x, \quad (20)$$

where $P(x,y_0)$ is an unknown function.

Similarly, the local transformation for $y_0 - \Delta y \le y \le y_0 + \Delta y$ for Eq. (19) is considered, this time, for $x = x_0$

$$J(x_0,y) = S(x_0,y)e^{[-q(x_0,y)]},\ \text{where } q\ (x_0,y) = -\frac{\mathrm{Re}}{2}\int_{y_0}^{y} v(x_0,y)\,dy \quad (21)$$

and $S(x_0,y)$ an unknown function.

Substitution of (20) to (18) and (21) to (19) gives the following system of equations

$$\frac{\partial^2 P}{\partial x^2} + \left(\frac{\mathrm{Re}}{2}\frac{\partial u}{\partial x} - \frac{\mathrm{Re}^2 u^2}{4}\right)P = [G_1(x,y_0) + A(x,y_0)]\mathrm{e}^{c(x,y_0)} \quad (22)$$

$$\frac{\partial^2 S}{\partial y^2} + \left(\frac{\mathrm{Re}}{2}\frac{\partial v}{\partial y} - \frac{\mathrm{Re}^2 v^2}{4}\right)S = -A(x_0,y)\mathrm{e}^{q(x_0,y)} \quad (23)$$

By discretizing equations using central-difference approximations at the point (x_0,y_0) for the second order derivatives of (22) and (23), eliminating $A(x_0,y_0)$, between the two new equations and substituting P and S by their appropriate expressions (20) and (21) at the corresponding points around (x_0,y_0), it is obtained that

$$J_1 e^{c_1} + J_3 e^{c_3} + \lambda^2 J_2 e^{q_2} + \lambda^2 J_4 e^{q_4} + \left(-2 + \frac{\mathrm{Re}\ (\Delta x)^2}{2}\left.\frac{\partial u}{\partial x}\right|_0 - \frac{\mathrm{Re}^{\ 2} u_0^2(\Delta x)^2}{4} - 2\lambda^2 + \frac{\mathrm{Re}\ (\Delta x)^2}{2}\left.\frac{\partial v}{\partial y}\right|_0 - \frac{\mathrm{Re}^2 v_0^2(\Delta x)^2}{4}\right)J_0$$
$$= (\Delta x)^2 G_1(x_0,y_0) + O((\Delta x)^4) + O((\Delta x)^2(\Delta y)^2), \quad (24)$$

where Δx and Δy is the Cartesian mesh size at the x and y direction, respectively and $\lambda = \Delta x/\Delta y$. The number of grid points is M and N at the x and y direction, respectively. By the subscripts 0, 1, 2, 3 and 4 it is denoted the typical set of grid points (x_0,y_0), $(x_0+\Delta x,y_0)$, $(x_0,y_0+\ \Delta y)$, $(x_0-\Delta x,y_0)$ and $(x_0,y_0-\Delta y)$, respectively.

However, the matrix of unknowns associated with (24) is not necessarily diagonally dominant, which is a prerequisite for the convergence of the iterative procedure. Diagonal dominance is obtained by expanding the exponential terms in Taylor series at the point (x_0,y_0) and keeping a sufficient number of terms so that the order of the truncation error is conserved.

Thus, $u(x,y)$ is expanded in Taylor series at the point (x_0,y_0) in the increasing direction of x, so that equation (20) can be integrated to give $c(x,y_0)$ in powers of $(x-x_0)$. The constants c_1 and c_3 are obtained in powers of Δx if in this latter equation is set successively $x = x_0 + \Delta x$ and $x = x_0 - \Delta x$, respectively.

The values of c_1 and c_3 are used for the calculation of e^{c_1} and e^{c_3} in the form of Taylor series, which will be substituted in the first two terms of the left-hand side of Eq. (24). The same procedure is followed to deduce likewise expressions for the other two terms of the left-hand side member of Eq. (24). In this way and using the equation of continuity (1), Eq. (17) finally takes the form

$$k_1 J_1 + k_2 J_2 + k_3 J_3 + k_4 J_4 + k_0 J_0 = (\Delta x)^2 G_1(x_0,y_0), \quad (25)$$

where

$$k_1 = 1 + \frac{\mathrm{Re}^2 u_0^2}{8}(\Delta x)^2 - \frac{\mathrm{Re} u_0}{2}(\Delta x),$$

$$k_2 = \lambda^2\left[1 + \frac{\mathrm{Re}^2 v_0^2}{8}(\Delta y)^2 - \frac{\mathrm{Re} v_0}{2}(\Delta y)\right],$$

$$k_0 = -2 - \frac{\mathrm{Re}^2 u_0^2(\Delta x)^2}{4} - 2\lambda^2 - \frac{\mathrm{Re}^2 v_0^2(\Delta x)^2}{4}$$

$$k_3 = 1 + \frac{\mathrm{Re}^2 u_0^2}{8}(\Delta x)^2 + \frac{\mathrm{Re} u_0}{2}\Delta x,$$

$$k_4 = \lambda^2\left[1 + \frac{\mathrm{Re}^2 v_0^2}{8}(\Delta y)^2 + \frac{\mathrm{Re} v_0}{2}(\Delta y)\right].$$

Similarly, for Eq. (12) and (14) it is obtained that

$$p_1\Psi_1 + p_2\Psi_2 + p_3\Psi_3 + p_4\Psi_4 + p_0\Psi_0 = -(\Delta x)^2 J_0, \quad (26)$$

where

$$p_1 = 1, \qquad p_2 = \lambda^2, \qquad p_3 = 1, \qquad p_4 = \lambda^2,$$
$$p_0 = -2 - 2\lambda^2.$$

$$d_1 T_1 + d_2 T_2 + d_3 T_3 + d_4 T_4 + d_0 T_0 = (\Delta x)^2 G_2(x_0, y_0), \quad (27)$$

where

$$G_2(x_0,y_0) = \mathrm{Mn}_M \mathrm{Pr}\ \mathrm{Ec} H^2\left\{\frac{\partial\Psi}{\partial y}\right\}^2 + \mathrm{Mn}_F \mathrm{Pr}\ \mathrm{Re}\ \mathrm{Ec}\ \mathrm{H}\ \varepsilon\left\{\frac{\partial H}{\partial x}\frac{\partial\Psi}{\partial y}\right\} + \mathrm{Pr}\ \mathrm{Ec}\left[\left(\frac{\partial^2\Psi}{\partial y^2} - \frac{\partial^2\Psi}{\partial x^2}\right)^2 + 4\left(\frac{\partial^2\Psi}{\partial x\partial y}\right)^2\right],$$

$$d_1 = 1 + \frac{\mathrm{Re}^2\ \mathrm{Pr}^2 u_0^2}{8}(\Delta x)^2 - \frac{\mathrm{RePr}\ u_0}{2}(\Delta x),$$

$$d_2 = \lambda^2\left[1 + \frac{\mathrm{Re}^2\ \mathrm{Pr}^2 v_0^2}{8}(\Delta y)^2 - \frac{\mathrm{RePr}\ v_0}{2}(\Delta y)\right],$$

$$d_0 = -2 - \frac{\mathrm{Re}^2\mathrm{Pr}^2 u_0^2(\Delta x)^2}{4} - 2\lambda^2 - \frac{\mathrm{Re}^2\mathrm{Pr}^2 v_0^2(\Delta x)^2}{4} - \mathrm{Mn}_F\mathrm{PrReEcH}\left\{\frac{\partial H}{\partial x}\frac{\partial\Psi}{\partial y}\right\}$$

$$d_3 = 1 + \frac{\mathrm{Re}^2\mathrm{Pr}^2 u_0^2}{8}(\Delta x)^2 + \frac{\mathrm{Re\ Pr}\ u_0}{2}\Delta x,$$

$$d_4 = \lambda^2\left[1 + \frac{\mathrm{Re}^2\mathrm{Pr}^2 v_0^2}{8}(\Delta y)^2 + \frac{\mathrm{Re\ Pr}\ v_0}{2}(\Delta y)\right].$$

The linear systems (25–27) are sparse and the matrices associated with them are always diagonally dominant since the coefficients of the unknowns satisfy the conditions [34]

$$\sum_{\substack{j=1\\ j\neq i}}^{N\times M}|k_{ij}| \le |k_{ii}|, \qquad \sum_{\substack{j=1\\ j\neq i}}^{N\times M}|m_{ij}| \le |m_{ii}|,$$

$$\sum_{\substack{j=1\\ j\neq i}}^{N\times M}|d_{ij}| \le |d_{ii}|, \quad i = 1,2,\ldots,N \times M$$

Equations (25–27) can be easily written in a way that constitutes a scalar tridiagonal system along each x grid line (i constant) and they are solved using the Thomas algorithm. It can be seen that this scheme is implicit, considering each i line constant, and therefore is called line by line implicit method (L.L.I.M.) [35]. The solution of the aforementioned equations is achieved iteratively, by solving, for all i lines, the arising tridiagonal systems until the unknown function at all the grid points of the computational domain has been evaluated up to an accuracy e.

The solution of the aforementioned system is obtained by using an iterative procedure. An over relaxation parameter equal to 1.2 was used for the L.L.I.M.

The steps of the procedure followed are

- Give initial guesses for the interior points of the computational domain and the boundary conditions.
- Calculate a new estimation for Ψ by solving (25) once, considering J known.
- Considering Ψ known construct the boundary conditions for J using (16).
- Calculate a new estimation for J by solving (26) using the L.L.I.M., considering Ψ, T known.
- Considering now Ψ and J known, calculate a new estimation for T using the L.L.I.M. for (27).
- Compare the new estimation with the old ones. If the criterion of convergence is not satisfied set the new estimations old and return to the second step.

The criterion of convergence used is

$$\frac{1}{MN}\sum_{i=1}^{M}\sum_{j=1}^{N}\left|F^{n+1} - F^{n}\right| < 10^{-5},$$

where F^n is an estimation of an unknown function F, (Ψ, J or T) at the n iteration.

5 Results and discussion

For the numerical solution of (12–14) it is necessary to assign values in the dimensionless parameters entering into the problem under consideration. For this purpose a realistic case is considered in which blood ($\bar{\rho} = 1050\ \mathrm{kg\ m^{-3}}$, $\bar{\mu} = 3.2 \times 10^{-3}\ \mathrm{kg\ m^{-1}s^{-1}}$) [36], flows with maximum velocity $\bar{u}_r = 1.828 \times 10^{-2}\mathrm{m\ s^{-1}}$ and the plates are located at distance $\bar{h} = 5.0 \times 10^{-2}$ m. In this case the Reynolds number, Re, is equal to 300. The temperature of the plates is $\bar{T}_{\mathrm{u}} = 42°\mathrm{C}$ and $\bar{T}_{\mathrm{l}} = 10.5°\mathrm{C}$. For these values of plate temperatures the temperature number $\epsilon = 9$.

The electrical conductivity $\bar{\sigma}$ of stationary blood was measured to be $0.7\ \mathrm{S\ m^{-1}}$ [24]. The electrical conductivity of flowing blood is always greater than that of the stationary. The increment for medium shear rates is about 10% and increases with the increment of the hematocrit [22]. In the current study the electrical conductivity of blood is assumed, for simplicity temperature independent, and equal to $0.8\ \mathrm{S\ m^{-1}}$.

Although the viscosity $\bar{\mu}$, the specific heat under constant pressure $\bar{c}_p$ and the thermal conductivity $\bar{k}$ of any fluid, and hence of blood, are temperature dependent, Prandtl number can be considered constant. Thus, for the temperature range considered in this problem,

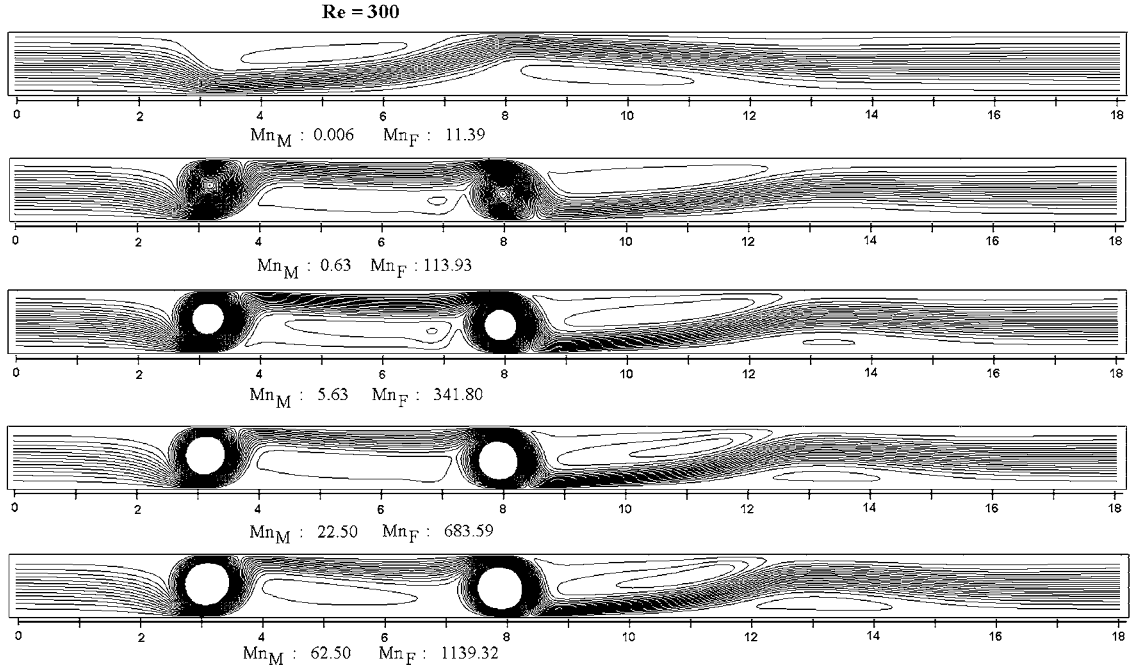

Fig. 4 Stream function contours for Re = 300 and for various values of Mn_M and Mn_F

the value of $\bar{c}_p$ and $\bar{k}$ is equal to 14.286 J kg $^{-1}$ K^{-1} and 1.832×10^{-3} J m^{-1} s^{-1} K^{-1}, respectively, [37] and hence the Prandtl number is taken equal to 25. For these values of the parameters the Eckert number is $\mathrm{Ec} = 7.43 \times 10^{-7}$.

The new dimensionless parameter appearing in the problem is the magnetic number Mn_F which can be written as

$$\mathrm{Mn}_F = \frac{\bar{\mu}_o \bar{H}_o^2 \bar{K}(\bar{T}_\mathrm{u} - \bar{T}_\mathrm{l})}{\bar{\rho}\bar{u}_r^2} = \frac{\bar{\mu}_o \bar{H}_o \bar{K} \bar{H}_o(\bar{T}_\mathrm{u} - \bar{T}_\mathrm{l})}{\bar{\rho}\bar{u}_r^2} = \frac{\bar{B}\bar{M}}{\bar{\rho}\bar{u}_r^2}, \quad (28)$$

where $\bar{B}$ and $\bar{M}$ are the magnetic induction and the magnetization, respectively. For magnetic field 8 Tesla, blood has reached magnetization of 40 A m^{-1} [14].

Using the definition of the Reynolds number, relation (28) becomes

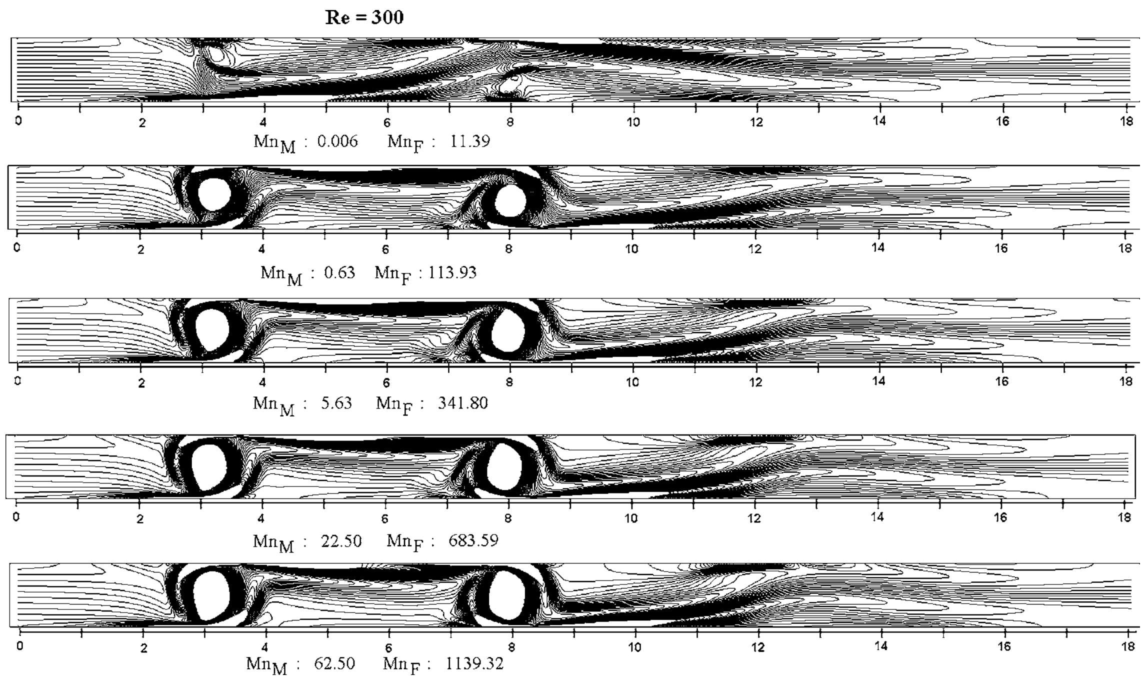

Fig. 5 Vorticity function contours for Re = 300 and for various values of Mn_M and Mn_F

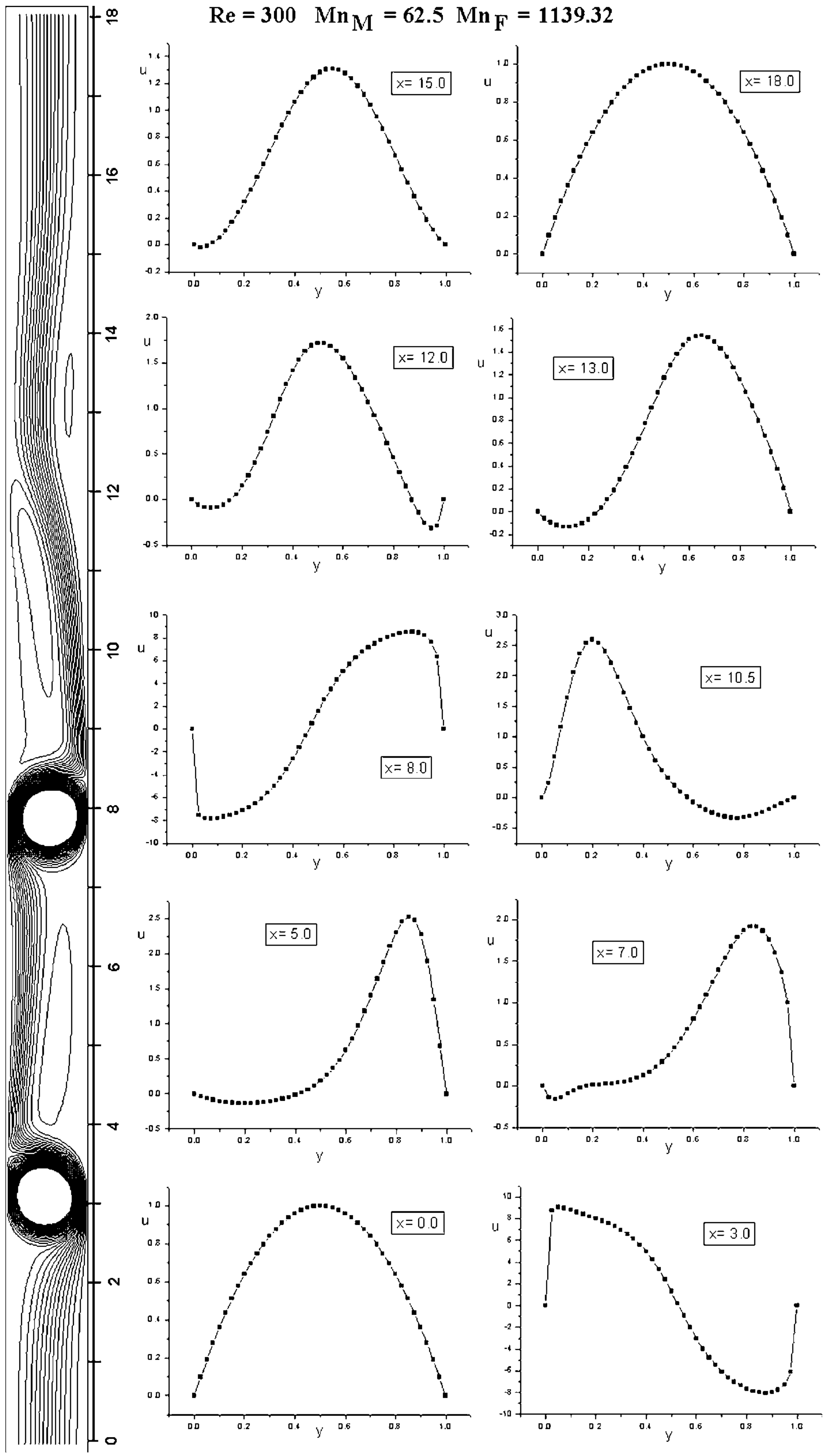

Fig. 6 Stream function contours and velocity profiles at various positions for $Mn_M = 62.5$, $Mn_F = 1139.32$ and $Re = 300$

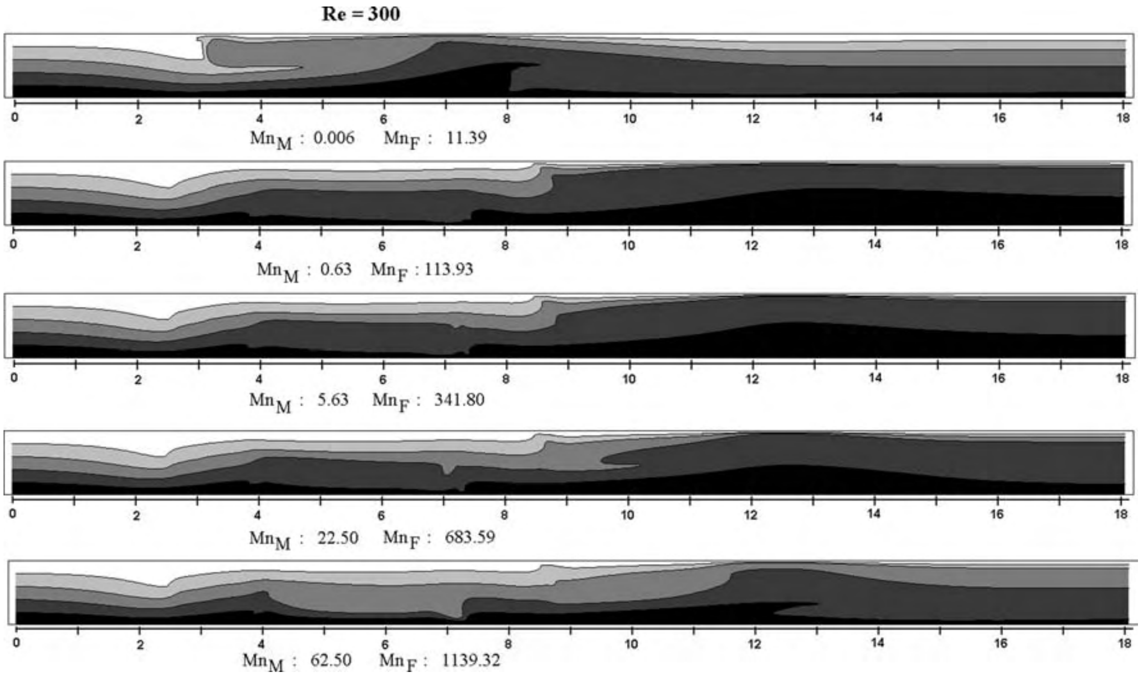

Fig. 7 Contours of the dimensionless temperature T for various values of Mn_M and Mn_F and for $\mathrm{Re} = 300$

$$\mathrm{Mn}_F = \frac{\bar{M}\bar{B}\bar{h}^2\bar{\rho}}{\bar{\mu}^2\ \mathrm{Re}^2}. \tag{29}$$

From Eq. (29) and the definition of the magnetic number Mn_M the following is obtained

$$\frac{\mathrm{Mn}_F}{\mathrm{Mn}_M} = \frac{\bar{\rho}\bar{M}}{\bar{\mu}\bar{B}\bar{\sigma}\ \mathrm{Re}^2} \approx \frac{2.051 \times 10^6}{\mathrm{Re}^2}. \tag{30}$$

Thus, for the problem under consideration where a magnetic field of 8 Tesla is assumed, the values of the magnetic numbers are $\mathrm{Mn}_F \approx 1139.323$ and $\mathrm{Mn}_M \approx 62.5$.

It is noted that the assumed magnetic field of 8 Tesla is considerably high and there may be practical problems in creating such a magnetic field. However, in many applications, especially in magnetic drug targeting, magnetic nanoparticles are injected in the blood in order to use them as a drug delivery system for localized therapy [3]. Similar nano-spheres have been constructed in order to increase the magnetization of blood [38]. These nano-spheres attach to the erythrocytes and as a consequence the magnetization of blood can be increased by one or two orders of magnitute. Thus, with the addition of magnetic nanoparticles in blood it is possible to achieve the same magnetic number Mn_F using magnetic field of order of 1T.

The length of the channel was chosen to be 18, whereas the magnetic field is applied between the points $x_1 = 3.0$, $x_2 = 8$ and the parameters a_1, a_2 appearing in (7) are both taken equal to 5. The present results where obtained for grid 701×41 at the x and y direction respectively, i.e. 28,741 grid points. Calculations where made also for 901×45, i.e. 45,951 grid points and no significant differences where found.

Figures 4, 5 show the stream and vorticity function contours, respectively, for the values of the above mentioned parameters and for various magnetic numbers. It is observed that the primary effect of the applied magnetic field is the formation of two vortices at the area of the points x_1 and x_2 between of which the magnetic field is applied. The first vortex rotates counterclockwise, whereas the second one clockwise. These two vortices are strengthened as the corresponding magnetic numbers are increased and they are formed even for very small magnetic numbers like $\mathrm{Mn}_F = 113.93$ (see Fig. 4). Between the two vortices and in the region where the magnetic field is applied one vortex is formed ($\mathrm{Mn}_F = 1139.32$, 683.59, 341.80, and 113.93). The ma gnetic field effects considerably the flow even for very low values of the magnetic field such as $\mathrm{Mn}_F = 11.39$, where only the two main vortices remain. Downstream the second vortex and outside the area where the magnetic field is applied, a relatively big vortex arises at the upper plate, whereas for relatively strong magnetic fields ($\mathrm{Mn}_F = 1139.32$, 683.59, and 341.80) a smaller one arises at the lower plate. The aforementioned smaller one vortex vanishes for relatively small magnetic fields (see Fig. 4).

The profiles of the dimensionless velocity component u along specific locations in the channel are shown in Fig. 6. From the profiles at $x = 3$ and 8 it is obtained that the first vortex rotates counterclockwise, whereas the second one clockwise. In the region where the magnetic field is applied, the biofluid is pressed to the upper plate due to the rotation direction of the two main vortices as it can be seen from the velocity profiles at $x = 5$ and 7. After the second major vortex and at

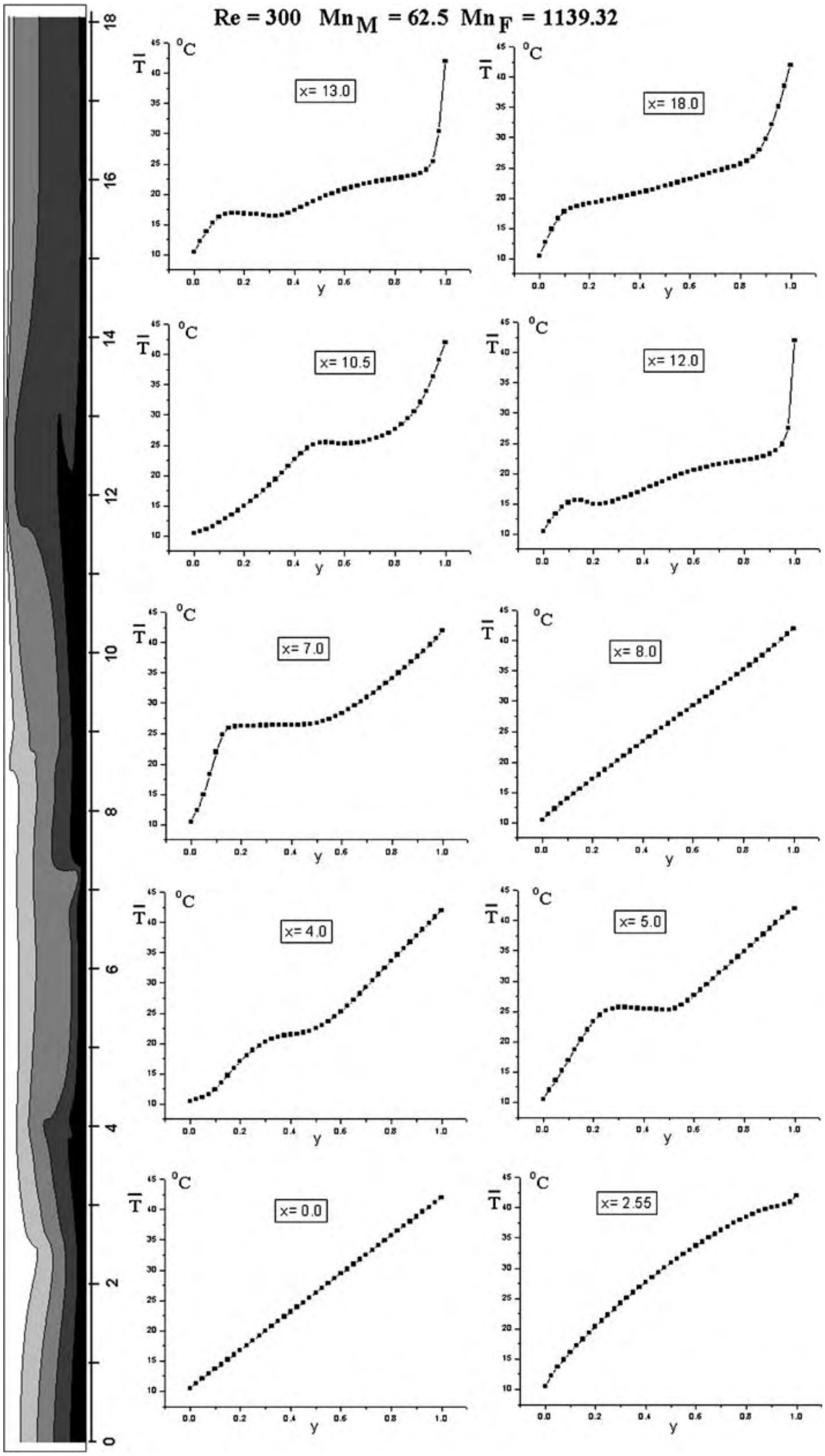

Fig. 8 Dimensional temperature contours and profiles at various positions for $\mathrm{Mn}_M = 62.5$, $\mathrm{Mn}_M = 1139.32$ and $\mathrm{Re} = 300$

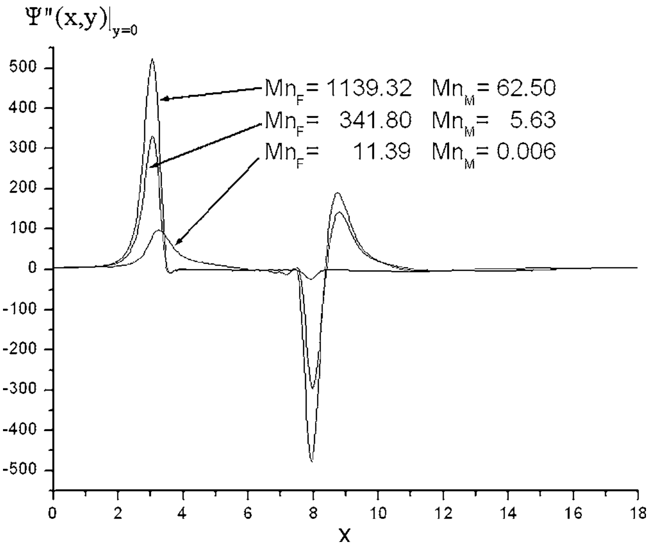

Fig. 9 Skin friction coefficient of the lower plate for Re = 300 and various magnetic numbers

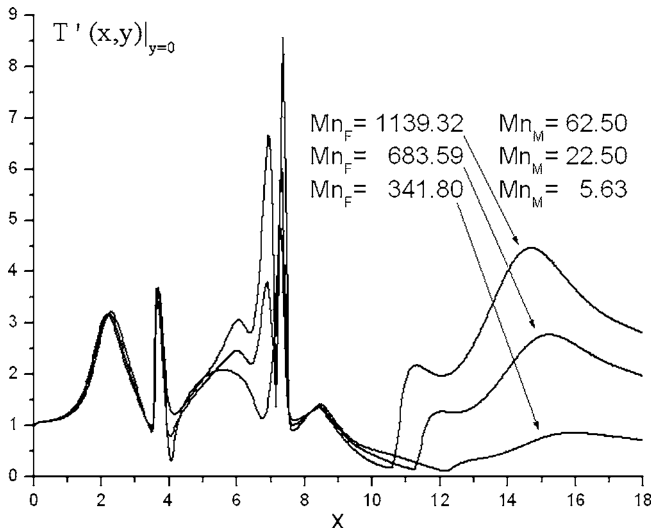

Fig. 11 Heat transfer parameter of the lower plate for Re = 300 and various magnetic numbers

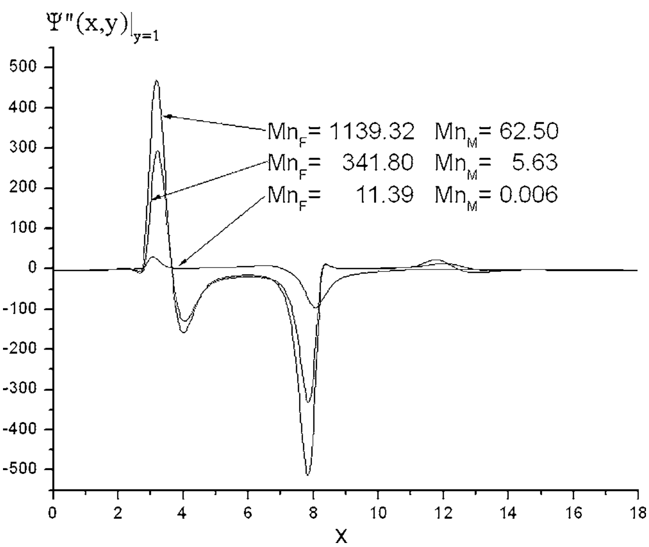

Fig. 10 Skin friction coefficient of the upper plate for Re = 300 and various magnetic numbers

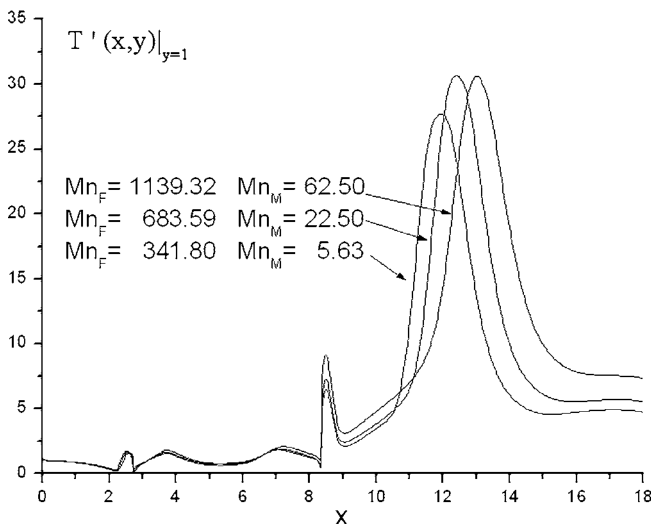

Fig. 12 Heat transfer parameter of the upper wall for Re = 300 and various magnetic numbers

$8.5 < x < 11.0$ the fluid is directed towards the lower plate (profile at $x = 10.5$) and another minor reverse of the flow takes place close to the lower plate and at $x = 13$. Finally, the flow at the exit ($x = 18$) is again reverted to fully developed.

It should be remarked that in the absence of the magnetic field (Mn = 0), the stream function as well as the vorticity function contours are straight lines and the velocity profile u is the same with the one shown at the entrance of the channel in Fig. 6.

The dimensionless temperature contours for the same values of the magnetic numbers are shown in Fig. 7. For $\mathrm{Mn}_F = 1139.32$ and $\mathrm{Mn}_M = 62.5$, the variation of the dimensional temperature $\bar{T}$ at different positions in the channel as well as the corresponding contours are shown in Figs. 8. It is observed that the dimensional temperature increases with greater rate, close to the lower plate, than that of the initial linear profile, from the point $x = 2.5$ until approximately the point $x = 8.0$. From this point until the exit of the channel, the dimensional temperature decreases with lower rate especially close to the upper plate ($y > 0.5$). In general, the dimensional temperature relatively (to the initial linear profile) increases with greater rate closer to the lower plate approximately at the area where the magnetic field is applied ($2.5 < x < 8.0$), whereas it increases with lower rate downstream the area where the magnetic field is applied.

The disturbance in the flow field due to the applied magnetic field is transferred very far downstream. As a result, the profile of the temperature at the exit of the channel differs from that at the entrance. Calculations

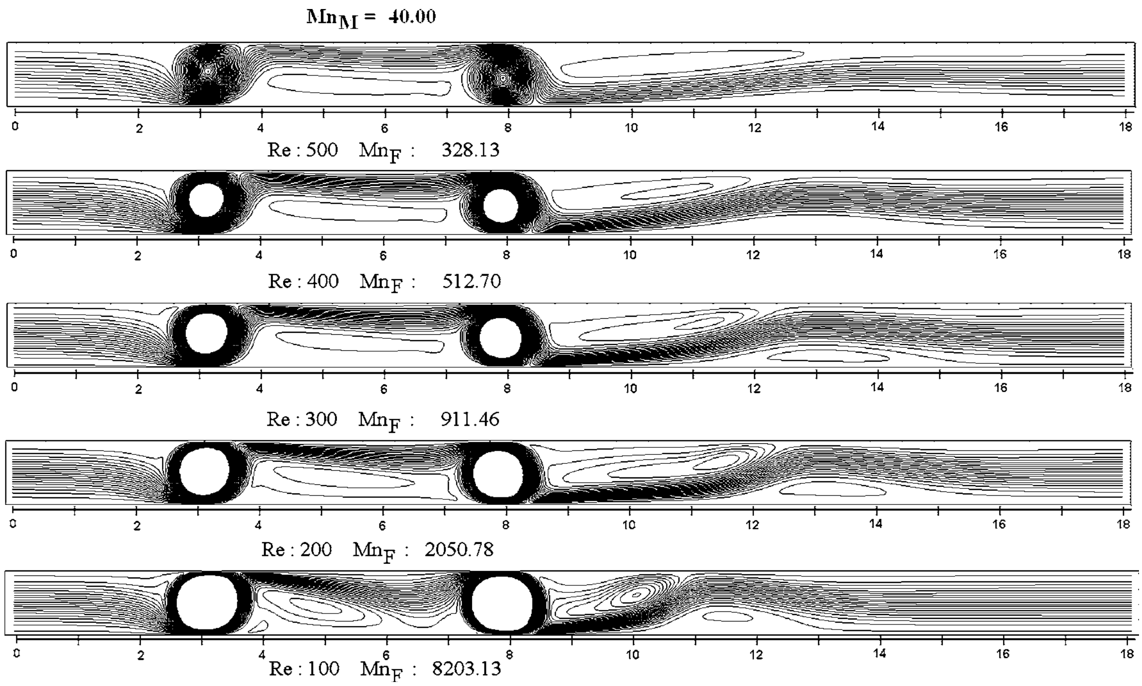

Fig. 13 Stream function contours for $\mathrm{Mn}_M = 40$ and for different values of Mn_F and Re

were made also for different grids and for $\bar{L}/\bar{h} = 25$ and 30 to verify this behavior. It is noted that in the absence of magnetic field the contours of the temperature are straight, equally spaced, lines.

The most important flow and heat transfer characteristics are the local skin friction coefficient and the local rate of heat transfer coefficient. These quantities can be defined by the following relations

$$C_f = \frac{2\bar{\tau}_l}{\bar{\rho}\bar{u}_r^2}, Nu = \frac{\bar{q}\bar{h}}{\bar{k}(\bar{T}_u - \bar{T}_l)}, \tag{31}$$

where, $\bar{\tau}_l = \bar{\mu}\left(\frac{\partial \bar{u}}{\partial \bar{y}}\right)\Big|_{\bar{y}=0,\bar{h}}$ is the wall shear stress and $\dot{\bar{q}} = -\bar{k}\left(\frac{\partial \bar{T}}{\partial \bar{y}}\right)\Big|_{\bar{y}=0,\bar{h}}$ is the heat flux between the fluid and the plates.

By using (8)–(11), the above mentioned quantities can be written as

$$C_f = \frac{2\Psi''(x,y)}{\mathrm{Re}}\bigg|_{y=0,1}, \ \mathrm{Nu} = \frac{\partial T}{\partial y}\bigg|_{y=0,1} = T'(x,y)|_{y=0,1}, \tag{32}$$

where Nu is the Nusselt number, $\Psi''(x,y)|_{y=0,1}$ is the dimensionless wall shear parameter and $T'(x,y)|_{y=0,1}$ is the dimensionless wall heat transfer parameter.

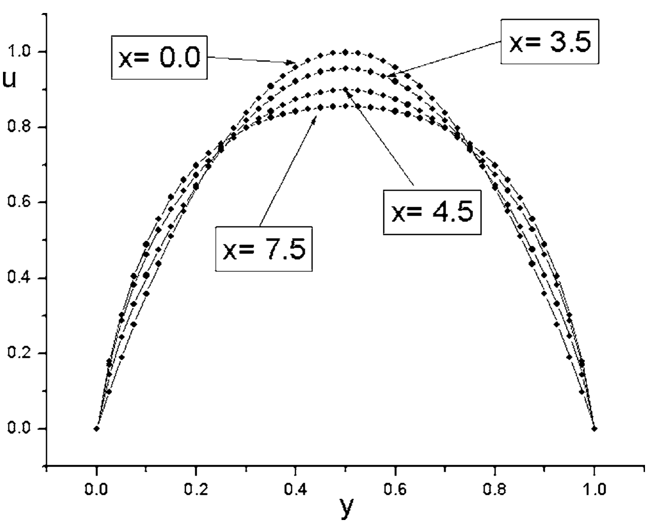

Fig. 14 Profiles of the dimensionless velocity u at various x positions

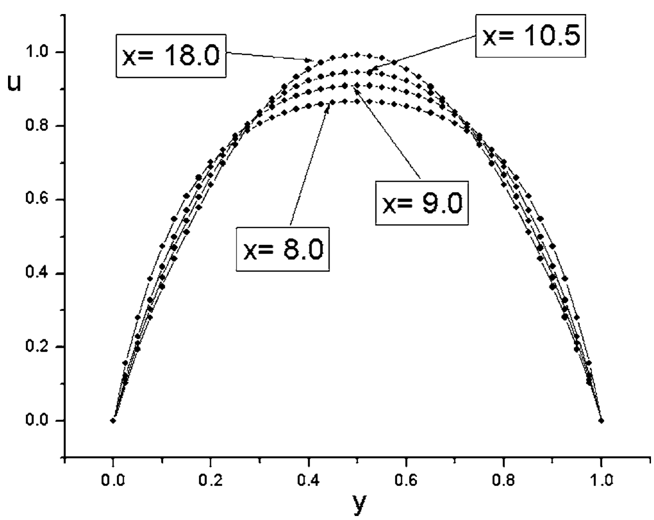

Fig. 15 Profiles of the dimensionless velocity u at various x positions

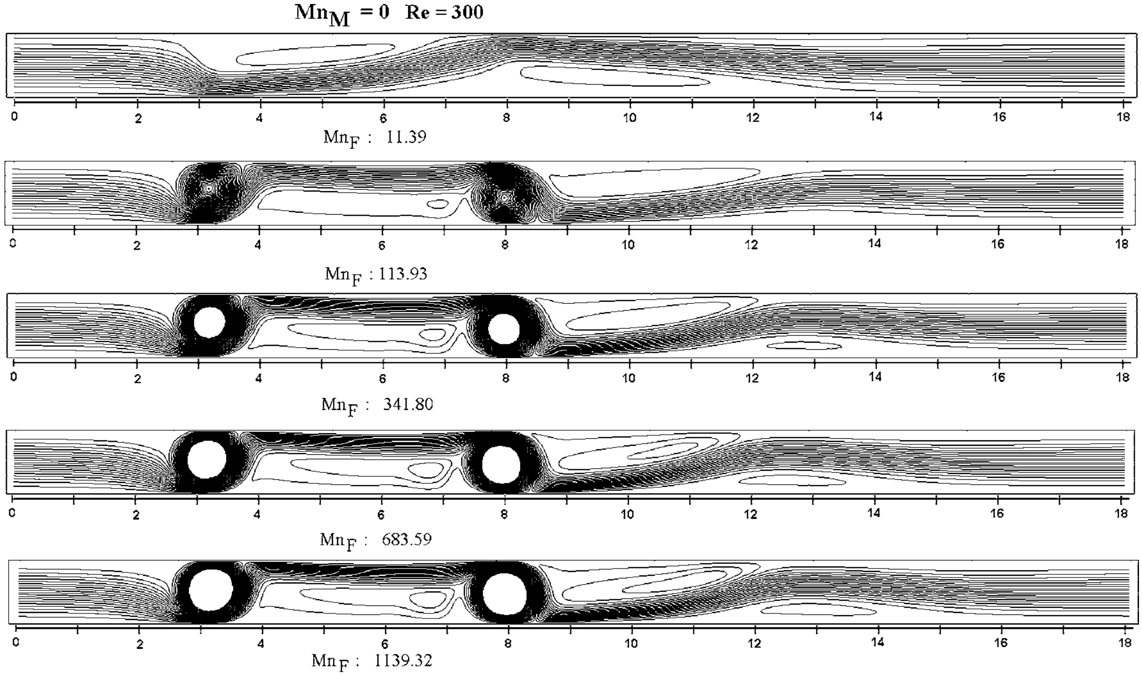

Fig. 16 Stream function contours for $\mathrm{Mn}_M = 0$ and $\mathrm{Re} = 300$ for various values of Mn_F

The variation of these dimensionless parameters, for $\mathrm{Mn}_F = 1139.32$, 341.80 and 11.39, are shown in Figs. 9–12. The wall shear parameters are more influenced at the points x_1 and x_2 between of which the magnetic field is applied. It is remarkable that the variation of each one of these parameters is qualitatively almost the same as the Mn_F varies from 11.39 to 1139.32. The increment of Mn_F results to greater variations of these parameters.

The dimensionless wall shear parameter of the lower plate, $\Psi''(x,y)|_{y=0}$, is pictured in Fig. 9 for the aforementioned values of Mn_F. The value of the parameter increases rapidly in the region $x = 2.0$ to $x = 3.0$, where it reaches its maximum value. From the point $x = 3.0$, where the magnetic field starts to apply, a corresponding decrement takes place and at $x = 3.5$ this parameter takes a value close to its original one. The next major variation takes place in the region $x = 7.5$ to $x = 10$. At the point $x = 7.5$ the value of the parameter starts to decrease rapidly and at the point $x = 8.0$, where the magnetic field stops, takes its minimum negative value. From the point $x = 8.0$ a rapid increment takes place and at the point $x \approx 8.8$ the parameter takes its maximum positive value. Finally, from the point $x \approx 8.8$ the parameter decreases and takes its original value of the fully developed flow.

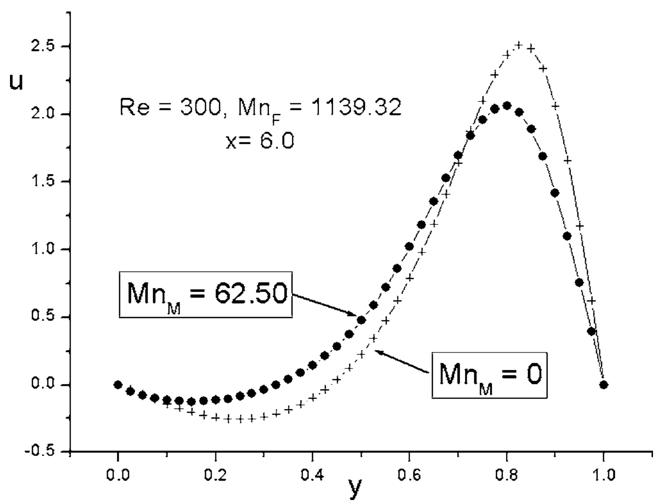

Fig. 17 Profiles of the dimensionless velocity u at $x = 6$ for $\mathrm{Re} = 300$, $\mathrm{Mn}_F = 1139.32$ and for $\mathrm{Mn}_M = 0$ and 62.5, respectively

Figure 10 shows the variation of the wall shear parameter of the upper plate, $\Psi''(x,y)|_{y=1}$, for the aforementioned values of Mn_F. This parameter varies similarly with the wall shear parameter of the lower plate as far as the major variations are concerned.

From Figs. 9 and 10 it can be observed that far downstream, $x > 16$, the wall shear parameter of both plates, reaches its original value (at $x = 0$) corresponding to the fully developed flow. The important information that can be obtained, is the points where these parameters take their maximum, minimum and zero values. At the points where the maximum or minimum value of the shear parameters of both plates is obtained, the skin friction is maximized whereas at the point where-these parameters are zero, the skin friction is zero and this result may be interesting in the case of creation of a fibrinoid.

Figures 11 and 12 show the variation of the heat transfer parameter for the lower and upper plate, respectively. For the lower plate (see Fig. 11) the parameter varies almost in the same way for $\mathrm{Mn}_F = 1139.32$, 683.59 and 341.80. The maximum values are attained at the points $x \approx 2.4,\ 3.8,\ 7.1$ and 14.5.

For the upper plate (see Figs. 12) the greater maximum, for all the considered magnetic numbers, is attained after the region of application of the magnetic field at about $11.5 < x < 13.5$. This behavior is justified by the presence of the large vortex at the upper plate at the same region (see Fig. 6). A second maximum, but much smaller than the previous one, appears at the point $x \approx 8.5$ just after the region where the magnetic field is applied. Far downstream the values of $T'(x, 0)$ or $T'(x, 1)$ do not reach their original values. This happens because, as already mentioned, the disturbance of the temperature field is extended far downstream.

As it can be seen from (30), the parameter Mn_F depends on the Reynolds number Re. From the definition of Mn_M it is also obtained that this number, for a specific problem ($\bar{h} = \bar{\rho} = \bar{\mu} =$ const) and magnetic field, is constant. Thus, if variation of Re number is considered due to the change of the velocity $\bar{u}_r$ at the entrance of the channel, Mn_F changes, whereas Mn_M remains constant. Figure 13 shows the contours of the stream function for $\mathrm{Mn}_M = 40.0$, which corresponds to magnetic field strength of 8 Tesla, and Reynolds numbers 500, 400, 300, 200, and 100. The corresponding Mn_F numbers are 328.13, 512.70, 911.46, 2050.78 and 8203.13, respectively. It is observed that as the Reynolds number decreases and the Mn_F number increases, the two vortices arise at the points where the magnetic field begins and ends to strengthen. As these vortices strengthen, the vortex arising at the upper plate, after the second major vortex, shrinks. For $\mathrm{Re} < 300$ the decrement in the extension of the later vortex leads also to the formation of one more minor vortex downstream at the lower plate.

As it was already mentioned, blood exhibits magnetization and also holds the property of an electrically conducting fluid. This happens mainly because of the tendency of erythrocytes to orient with the applied magnetic field (magnetization) and the appearance of ions in the plasma (electrical conductivity). Most of the biofluids due to the existing ions in the body may be influenced by the magnetic field only due to their electrical conductivity. In order to study the effect of the magnetic field due only to the electrical conductivity it is possible to set Mn_F zero, and let Mn_M vary. If the opposite is done then it is possible to study the effect of the magnetic field due to the magnetization of the fluid.

Figures 14 and 15 show the velocity profiles for different positions in the channel for $\mathrm{Mn}_F = 0$, $\mathrm{Mn}_M = 40.0$ and $\mathrm{Re} = 300$. The velocity profiles start from the entrance ($x = 0$) and for $x = 3.5,\ 4.5,\ 7.5$. It is apparent that the maximum value of the velocity reduces as the biofluid enters the area where the magnetic field is applied. In the same manner, the maximum value of the velocity takes gradually its initial value of the fully developed flow as the biofluid leaves the area of application of the magnetic field (see Fig. 15).

Stream function contours for $\mathrm{Mn}_M = 0$ (non conducting biofluid), $\mathrm{Re} = 300$ and for various Mn_F numbers are pictured in Figs. 16. It is obtained after comparison with Fig. 4, where the electrical conductivity is additionally taken into account, that the Lorentz force affects the area between the two vortices for relatively high Mn_F numbers. For $\mathrm{Mn}_F = 341.80$ the stream function contours are almost the same and for lower values of Mn_F ($= 113.93$ and 11.39) the stream function contours are identical to the corresponding ones of Fig. 4.

Two representative velocity profiles at $x = 6$, for $\mathrm{Mn}_F = 1139.32$ are shown in Fig. 17 for $\mathrm{Mn}_M = 0$ and 62.50, respectively. The difference of the profiles taking into account the electrical conductivity of blood is considerable. It is obtained that the variations in the velocity profile (maximum and minimum values) decrease as the electrical conductivity is taken into account.

Thus, the electrical conductivity of blood cannot be ignored as it is proposed by the model of Haik et. al. [4, 13, 14] for relatively strong magnetic fields in the area where the magnetic field is uniform. At the areas where the magnetic field gradient exists (in our case at the areas of $x = 3$ and $x = 8$) the contribution of the electrical conductivity is negligible and the model of FHD is a very good approximation.

The above mentioned results indicate that the application of a magnetic field, in the flow of a biomagnetic fluid should be further studied for possible useful medical and engineering applications.

6 Conclusions

The simplified fundamental problem of the biomagnetic (blood) fluid flow in a channel under the influence of a strong, steady, uniform, locally applied, magnetic field is studied. The numerical solution of the problem is obtained by the development of an efficient numerical technique based on finite differences. This technique assures that in the algebraic system arising after discretization, the matrix of the unknowns is diagonally dominant. From the numerical investigation it is obtained that the electrical conductivity of blood should be taken into account at the area of the uniform magnetic field. At the two points, where the magnetic field starts and stops to apply, the magnetic field gradient is high and the assumption that blood is an electrically non–conducting fluid is a very good approximation. From the results concerning the velocity and temperature field, skin friction and rate of heat transfer, it is obtained that in general the magnetic field influences considerably the flow field causing the formation of two vortices at the area of the two points where the magnetic field starts and stops to apply.

Acknowledgment This work was partially supported by the No. 2439 Karatheodoris program of the Research Committee University of Patras.

References

1. Carlton JMR, Yowell CA, Sturrock KA, Dame JB (2001) Biomagnetic separation of contaminating host leukocytes from plasmodium-infected erythrocytes. Exp Parasitol 97:111–114
2. Fuh CB, Lin LY, Lai MH (2000) Analytical magnetapheresis of magnetically susceptible particles. J Chromatogr A 874:131–142
3. P.A. Voltairas, D.I. Fotiadis, L.K. Michalis (2002) Hydrodynamics of magnetic drug targeting. J Biomechanics 35:813–821
4. Haik Y, Pai V, Chen CJ (1999) Development of magnetic device for cell separation. J Magnetism Magn Mate 194:254–261
5. Badescou V, Rotariu O, Murariu V, Rezlescu N (1997) Transverse high gradient magnetic filter cell with bounded flow field. IEEE Trans Magn 33(6):4439–4444
6. Ruuge EK, Rusetski AN (1993) Magnetic fluid as drug carriers: Targeted transport of drugs by a magnetic field. J Magnetism Magn Mate 122:335–339
7. Plavins J, Lauva M (1993) Study of colloidal magnetite binding erythrocytes: Prospects for cell separation. J Magnetism Magn Mate 122:349–353
8. Pauling L, Coryell CD (1936) The magnetic Properties and Structure of Hemoglobin, Oxyhemoglobin and Carbonmonoxy Hemoglobin. In: Proceedings of the National Academy of Science, USA 22:210–216
9. Higashi T, Yamagishi A, Takeuchi T, Kawaguchi N, Sagawa S, Onishi S, Date M (1993) Orientation of erythrocytes in a strong static Magn field. J Blood 82(4):1328–1334
10. Shaylgin AN, Norina SB, Kondorsky EI (1983) Behavior of erythrocytes in high gradient magnetic field. J Magnetism Magn Mate 31:555–556
11. Takeuchi T, Mizuno T, Yamagishi A, Higashi T, Date M (1995) Orientation of red blood cells in high magnetic field. J Magnetism and Magn Mate 2(140–144):1462–1463
12. Higashi T, Ashida N, Takeuchi T (1997) Orientation of blood cells in static magnetic field. Physica B 616–620
13. Haik Y, Chen JC, Pai VM (1996) Development of bio-magnetic fluid dynamics. In: Proceedings of the IX International Symposium on Transport Properties in Thermal Fluids Engineering, Singapore, Pacific Center of Thermal Fluid Engineering, Winoto SH, Chew YT, Wijeysundera NE, (eds) Hawaii, USA., June 25–28:121–126
14. Haik Y, Pai V, CJ Chen (1999) Biomagnetic Fluid Dynamics. In: Fluid dynamics at interfaces, Shyy W, Narayanan R (eds) Cambridge University Press London, 439–452
15. Bashtovoy VG, Berkovsky BM, Vislovich AN (1998) Introduction to thermomechanics of magnetic fluids. Hemisphere publishing co., Springer-Verlag
16. Berkovski B, Bashtovoy V (1996) Magnetic fluids and applications handbook. Begell house inc., New York
17. Blums E, Cebers A, Maiorov MM (1997) Magnetic fluids. Walter de Gruyter, Berlin
18. Fertman VE (1990) Magnetic fluids guidebook: properties and applications. Hemisphere publishing co., New York
19. Neuringer JL, Rosensweig RE (1964) Ferrohydrodynamics. Phys Fluids 7:1927–1937
20. Rosensweig RE (1985) Ferrohydrodynamics. Cambridge University Press
21. Rosensweig RE (1987) Magnetic fluids. Ann Rev Fluid Mech 19:437–463
22. Frewer RA (1974) The electrical conductivity of flowing blood. Biomed Eng 552–554
23. Jaspard F, Nadi M (2002) Dielectric properties of blood: an investigation of temperature dependence. Physiol Meas 23:547–554
24. Gabriel S, Lau RW, Gabriel C (1996) The dielectric properties of biological tissues: III. Parametric models for the dielectric spectrum of tissues. Phys Medicine Biol 41:2271–2293
25. Cramer KR, Pai SI (1973) Magnetofluid dynamics for engineers and applied physicists. Scripta Publishing Company, Washington D.C
26. Hughes WF, Young FJ (1996) The electromagnetodynamics of fluids. 1st edn. Wiley Inc. New York
27. Sutton GW, Sherman A (1965) Engineering magnetohydrodynamics. McGraw-Hill, Inc. New York
28. Zendehbudi GR, Moayeri MS (1999) Comparison of physiological and simple pulsatile flows through stenosed arteries. J Biomech 32:959–965
29. Andersson HI, Halden R, Glomsaker T (2000) Effects of surface irregularities on flow resistance in differently shaped arterial stenoses. J Biomech 33(10):1257–1262
30. Matsuki H, Yamasawa K, Murakami K (1977) Experimental Considerations on a new Automatic Cooling Device Using Temperature Sensitive Magnetic Fluid. IEEE Trans Magn 13(5):1143–1145
31. Loukopoulos V, Tzirtzilakis E (2004) Biomagnetic channel flow in spatially varying magnetic field. Int J Eng Sci 42:571–590
32. Loukopoulos VC (2002) A Difference Method for Solving the Navier–Stokes Equations for Axisymmetric Flow. In: Proceedings of 4th GRACM Congress on Computational Mechanics, Patras, Greece 1:88–95
33. Loukopoulos VC, Katsiaris GA, Karahalios GT (2003) A steady–state solver for the simulation of Taylor vortices in spherical annular flow. Computer methods in Applied Mech Eng 192:2993–3003
34. Atkinson K (1992) An introduction to numerical analysis. John Wiley & Sons, New York
35. Patankar S (1980) Numerical heat transfer and fluid flow. Hemisphere Publishing Corporation
36. Pedley TJ (1980) The fluid mechanics of large blood vessels. Cambridge University Press
37. Chato JC (1980) Heat tranfer to blood vessels. J. Biomech Eng 102:110–118
38. Haik Y, Chen CJ, Chatterjee J (2002) Numerical simulation of biomagnetic fluid in a channel with thrombus. J Visualization 5(2):187–195